Jefferson Lab PAC24

Proposal Cover Sheet

This document must be received by close of business Thursday, April 28, 2003 at:

Jefferson Lab
User Liaison,
Mail Stop 12B
12000 Jefferson Ave.
Newport News, VA
23606

Experimental Hall: A

Days Requested for Approval: 28

❒ Proposal Title:

Measurement of the Neutron d_2: Towards the Electric χ_E and Magnetic χ_B Color Polarizabilities

Proposal Physics Goals

Indicate any experiments that have physics goals similar to those in your proposal.

Approved, Conditionally Approved, and/or Deferred Experiment(s) or proposals:

E94-010, E97-103, E99-117, E01-012 and E01-006

Contact Person

Name: Zein-Eddine Meziani
Institution: Temple University
Address: Department of Physics, Barton Hall A323
Address: 1900 North 13th Street
City, State, ZIP/Country: Philadelphia, PA, 19122/USA
Phone: (215) 204-5971 Fax: (215) 204-2569
E-Mail: meziani@temple.edu

Jefferson Lab Use Only

Receipt Date:_____

By:_____

BEAM REQUIREMENTS LIST

JLab Proposal No.: _____ Date: 04/28/2003

Hall: A Anticipated Run Date: _____ PAC Approved Days: _____

Spokesperson: S. Choi, X. Jiang, Z.-E. Meziani Hall Liaison: J. P. Chen
Phone: (215) 204 5971, (757) 269 7011
E-mail: meziani@temple.edu

List all combinations of anticipated targets and beam conditions required to execute the experiment. (This list will form the primary basis for the Radiation Safety Assesment Document (RSAD) calculations that must be performed for each experiment.)

Condition No.	Beam Energy (MeV)	Mean Beam Current (μA)	Polarization and Other Special Requirements (e.g., time structure)	Target Material (use multiple rows for complex targets — e.g., w/windows)	Material Thickness (mg/cm^2)	Est. Beam-On Time for Cond. No. (hours)
1	6000.	15.	Polarization 80%	^{3}He	50	10
	6000.	15.		Glass window	44	
2	5700.	15.	Polarization 80%	^{3}He	50	2
	5700.	15.		Glass window	44	

The beam energies, E_{Beam}, available are: $E_{Beam} = N \times E_{Linac}$ where N = 1, 2, 3, 4, or 5. $E_{Linac} = 800$ MeV, i.e., available E_{Beam} are 800, 1600, 2400, 3200, and 4000 MeV. Other energies should be arranged with the Hall Leader before listing.

HAZARD IDENTIFICATION CHECKLIST

JLab Proposal No.: _____ Date: 04/28/2003
(For CEBAF User Liaison Office use only.)

Check all items for which there is an anticipated need.

Cryogenics
_____ beamline magnets
_____ analysis magnets
_____ target
type: _____
flow rate: _____
capacity: _____

Electrical Equipment
_____ cryo/electrical devices
_____ capacitor banks
_____ high voltage
_____ exposed equipment

Radioactive/Hazardous Materials
List any radioactive or hazadorous/ toxic materials planned for use:
_____
_____
_____
_____

Pressure Vessels
19 mm inside diameter
13 atm operating pressure
Glass window material
~100 μm window thickness

Flammable Gas or Liquids
type: _____
flow rate: _____
capacity: _____

Drift Chambers
type: _____
flow rate: _____
capacity: _____

Other Target Materials
___ Beryllium (Be)
___ Lithium (Li)
___ Mercury (Hg)
___ Lead (Pb)
___ Tungsten (W)
___ Uranium (U)
X Other (list below)
^{3}He, N_2 and Rb
_____

Vacuum Vessels
_____ inside diameter
_____ operating pressure
_____ window material
_____ window thickness

Radioactive Sources
_____ permanent installation
_____ temporary use
type: _____
strength: _____

Large Mech. Structure/System
_____ lifting devices
_____ motion controllers
_____ scaffolding or
_____ elevated platforms

Lasers
type: Laser diode system
wattage: 7x30 W
class: IV

Installation:
X permanent*
_____ temporary
* for this experiment

Use:
_____ calibration
_____ alignment

Hazardous Materials
____ cyanide plating materials
____ scintillation oil (from)
____ PCBs
____ methane
____ TMAE
____ TEA
____ photographic developers
____ other (list below)
_____
_____

General:
Experiment Class:

X Base Equipment
_____ Temp. Mod. to Base Equip.
_____ Permanent Mod. to Base Equipment
_____ Major New Apparatus

Other: Polarized ^{3}He target with Laser Hut

Computing Requirements List

Proposal Title: Measurement of the Neutron d2 Matrix Element: Towards the Electric and Magnetic Color Polarizabilities

Spokesperson: S. Choi, X. Jiang, Z.-E. Meziani

Experimental Hall: A

Raw Data Expected

Total: 3000 GB

Per Year (long duration experiments only):

Simulation Compute Power (SPECint95 hours) Required: N/A

On-Line Disk Storage Required: 200 GB

Imported Data Amount from Outside Institutions: N/A

Exported Data Amount to Outside Institutions: N/A

Expected Mechanism for Imported/Exported Data: N/A

Special Requirements

For example, special configuration of data acquisition systems) that may require resources and/or coordination with JLab's Computer Center. Please indicate, if possible, what fraction of these resources will be provided by collaborating institutions and how much is expected to be provided by JLab.

Measurement of the Neutron d_2: Towards the Electric χ_E and Magnetic χ_B Color Polarizabilities

X. Zheng
Argonne National Laboratory, Argonne, IL 60439, USA

P. Bertin
Université Blaise Pascal De Clermont-Ferrand, Aubiere 63177, France

J.-P. Chen, E. Chudakov, C. W. de Jager, R. Feuerbach, J. Gomez, J. -O. Hansen, D.W. Higinbotham, J. LeRose, W. Melnitchouk, R. Michaels, S. Nanda, A. Saha, B. Reitz, B. Wojtsekhowski
Jefferson Lab, Newport News, VA 23606, USA

S. Frullani, F. Garibaldi, M. Iodice, G. Urciuoli, F. Cusanno
Istituto Nazionale di Fiscica Nucleare, Sezione Sanità, 00161 Roma, Italy

R. DeLeo, L. Lagamba
Istituto Nazionale di Fiscica Nucleare, Bari, Italy

A.T. Katramatou, G.G. Petratos
Kent State University, Kent, OH 44242

W. Korsch
University of Kentucky, Lexington, KY 40506, USA

W. Bertozzi, Z. Chai, S. Gilad, M. Rvachev, Y. Xiao
Massachusetts Institute of Technology, Cambridge, MA 02139, USA

L. Gamberg
Penn State Berks, Reading, PA, 19610 USA

F. Benmokhtar, R. Gilman, C. Glashausser, K. McCormick, X. Jiang (co-spokesperson), G. Kumbartzki, R. Ransome
Rutgers University, Piscataway, NJ 08855, USA

Seonho Choi(co-spokesperson), F. Butaru, A. Lukhanin, Z.-E. Meziani (co-spokesperson), K. Slifer, P. Solvignon, H. Yao
Temple University, Philadelphia, PA 19122, USA

S. Binet, G. Cates, A. Deur, N. Liyanage, J. Singh, A. Tobias
University of Virginia, Charlottesville, VA 22901, USA

T. Averett, J. M. Finn, D. Armstrong, K. Griffioen, K. Kramer, V. Sulkosky, J. Roche
College of William and Mary, Williamsburg, VA 23185, USA

and the

Hall A COLLABORATION

April 28, 2003

Contact: Z.-E. Meziani (meziani@temple.edu)

Abstract

We propose to make a measurement of the spin-dependent scattering cross section for a longitudinally polarized electron beam off a transversely and longitudinally polarized ^{3}He target. This measurement will cover excitation energies across the resonance and deep inelastic regions at constant 4-momentum transfer $Q^2 = 2$ (GeV/c)^2. We will extract the quantity $d_2^n = \int_0^1 x^2(2g_1 + 3g_2)\ dx$ and $\Gamma_2^n = \int_0^1 g_2\ dx$. This measurement will significantly improve the precision of the neutron d_2 world data and test the predictions of several models including the lattice QCD calculation of this quantity. Furthermore, the Burkhardt-Cottingham sum rule will be tested at $Q^2 = 2$ (GeV/c)^2. The quantity d_2^n reflects the response of the color electric and magnetic fields to the polarization of the nucleon. Because d_2^n is a higher moment of structure functions it is dominated by the contributions from the large x region. CEBAF at Jefferson Lab is ideal to perform such a measurement.

1 Introduction and Motivation

In inclusive polarized lepton-nucleon deep-inelastic scattering, one can access two spin-dependent structure functions of the nucleon, g_1 and g_2. While g_1 can be understood in terms of the Feynman parton model which describes the scattering in terms of *incoherent* parton scattering, g_2 cannot. Rather, one has to consider parton correlations initially present in the participating nucleon, and the associated process is given a *coherent* parton scattering in the sense that more than one parton takes part in the scattering. Indeed, using the operator product expansion (OPE) [1, 2], it is possible to interpret the g_2 spin structure function beyond the simple quark-parton model as a higher twist structure function. . As such, it is exceedingly interesting because it provides a unique opportunity to study the quark-gluon correlations in the nucleon which cannot otherwise be accessed.

In a recent review Ji [3] explained that higher-twist processes cannot be cleanly separated from the leading twist because of the so-called infrared renormalon problem first recognized by t' Hooft. This ambiguity arises from separating quarks and gluons pre-existing in the hadron wave function from those produced in radiative processes. Such a separation turns out to be always scheme dependent. Nevertheless, the g_2 structure function is an **exception** because it contributes at the leading order to the spin asymmetry of longitudinally-polarized lepton scattering on transversely-polarized nucleons. Thus, g_2 is among the *cleanest* higher-twist observables.

Why does the g_2 structure function contain information about the quark and gluon correlations in the nucleon? According to the optical theorem, g_2 is the imaginary part of the spin-dependent Compton amplitude for the process $\gamma^*(+1) + N(1/2) \to \gamma^*(0) + N(-1/2)$,

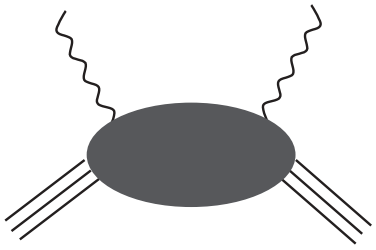

Figure 1: Compton amplitude of $\gamma^*(+1) + N(1/2) \to \gamma^*(0) + N(-1/2)$.

where γ^* and N denote the virtual photon and the nucleon, respectively, and the numbers in the brackets are the helicities. Thus this Compton scattering involves the t-channel helicity exchange $+1$. When it is factorized in terms of parton sub-processes, the intermediate partons must carry this helicity exchange. Because of the chirality conservation in vector coupling, massless quarks in perturbative processes cannot produce a helicity flip. Nevertheless, in QCD this helicity exchange may occur in the following two ways (see Fig. 2): first, single quark scattering in which the quark carries one unit of orbital angular momentum through its transverse momentum wave function; second, quark scattering with an additional transversely-polarized gluon from the nucleon target. The two mechanisms are combined in such a way to yield a gauge-invariant result. Consequently, g_2 provides a direct probe of the quark-gluon correlations in the nucleon wave function.

1.1 The twist-three reduced matrix element

The piece of interesting physics we want to focus on in this proposal is contained in the second moment in x of a linear combination of g_1 and g_2, namely

$$d_2(Q^2) \;=\; \int_0^1 x^2[2g_1(x,Q^2) + 3g_2(x,Q^2)]dx \tag{1}$$

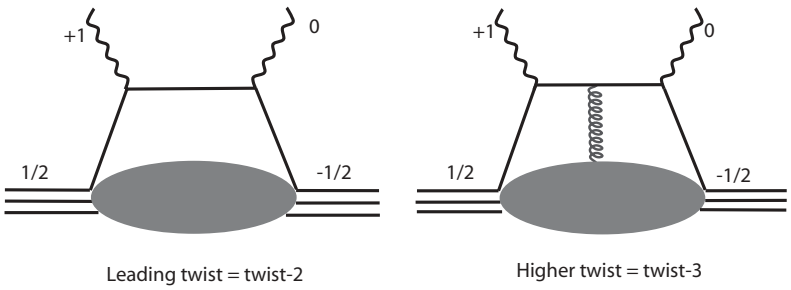

Figure 2: Twist-two and twist-three contributions to virtual Compton scattering

$$= \quad 3\int_0^1 x^2\Big[g_2(x,Q^2) - g_2^{WW}(x,Q^2)\Big]dx$$

where g_2^{WW}, known as the Wandzura-Wilczek [13] term, depends only on g_1

$$g_2^{WW}(x,Q^2) = -g_1(x,Q^2) + \int_x^1 \frac{g_1(y,Q^2)}{y}dy. \tag{2}$$

It is interesting to see that the quantity d_2 also appears in the first moment of g_1 when at large Q^2 ($Q^2 \gg \Lambda^2_{QCD}$) it is expressed in terms of a twist expansion [10, 11]:

$$\Gamma_1(Q^2) = \int_0^1 g_1(Q^2,x)dx = \frac{1}{2}a_0 + \frac{M^2}{9Q^2}\Big(a_2 + 4d_2 + 4f_2\Big) + O\Big(\frac{M^4}{Q^4}\Big), \tag{3}$$

where a_0 is the leading twist, dominant contribution. It is determined, apart from QCD radiative corrections [12], by the triplet g_A and octet a_8 axial charges and the net quark spin contribution to the total nucleon spin. These axial charges are extracted from measurements of the neutron and hyperons weak decay measurements [14]. Here a_2 is a second moment of the g_1 structure function and arises from the target mass correction [11]. The quantities d_2 and f_2 are the twist-three and the twist-four reduced matrix elements. These matrix elements contain non-trivial quark gluon interactions beyond the parton model. A first attempt at extracting f_2 has been carried by Ji and Melnitchouk in [17] using the world data but with poor statistics below $Q^2 = 1$ GeV^2. Other investigations of higher twist contributions for spin-dependent structure functions were performed and reported in Ref. [18, 19]. In QCD, d_2 and f_2 can be expressed as linear combinations of the induced color electric and magnetic polarizabilities χ_E and χ_B [3, 16] when a nucleon is polarized. The above twist expansion may be valid down to $Q^2 \approx 1$ GeV^2 if higher order terms are small.

At large Q^2 where an OPE expansion becomes valid, the quantity d_2 reduces to a twist-3 matrix element which is related to a certain quark-gluon correlation.

$$\langle PS|\frac{1}{4}\bar{\psi}g\tilde{F}^{\sigma(\mu}\gamma^{\nu)}\psi|PS\rangle = 2d_2 S^{[\sigma}P^{(\mu]}P^{\nu)} \ , \tag{4}$$

where $\tilde{F}^{\mu\nu} = (1/2)\epsilon^{\mu\nu\alpha\beta}F_{\alpha\beta}$, and $(\cdots)$ and $[\cdots]$ denote symmetrization and antisymmetrization of indices, respectively. The structure of the above operator suggests that it measures a quark *and* a gluon amplitude in the initial nucleon wavefunction [1, 2].

The physical significance of $d_2(Q^2)$ has been articulated by Ji and we quote, "*we ask when a nucleon is polarized in its rest frame, how does the gluon field inside of the nucleon respond?*

Intuitively, because of the parity conservation, the color magnetic field $\vec{B}$ can be induced along the nucleon polarization and the color electric field $\vec{E}$ in the plane perpendicular to the polarization". After introducing the color-singlet operators $O_B = \psi^\dagger g\vec{B}\psi$ and $O_E = \psi^\dagger\vec{\alpha}\times g\vec{E}\psi$, we can define the gluon-field polarizabilities χ_B and χ_E in the rest frame of the nucleon,

$$\langle PS|O_{B,E}|PS\rangle = \chi_{B,E} 2M^2\vec{S} \ . \tag{5}$$

Then d_2 can be written as

$$d_2 = (\chi_E + 2\chi_B))/8 \ . \tag{6}$$

Thus d_2 is a measure of the response of the color electric and magnetic fields to the polarization of the nucleon. The reduced matrix element f_2 can be expressed also as a different linear combination of the same color polarizabilities

$$f_2 = (\chi_E - \chi_B)/3 \ . \tag{7}$$

Ultimately from $d_2(Q^2)$ and $f_2(Q^2)$ the color electric and magnetic polarizabilities will be obtained when high precision data on both g_1 and $g_2$of both quantities become available. In this proposal we are aiming at providing precision data for d_2^n at large Q^2.

1.2 Burkhardt-Cottingham Sum rule

The g_2 structure function itself obeys the Burkhardt-Cottingham (BC) sum rule [21]

$$\Gamma_2(Q^2) = \int_0^1 g_2(x,Q^2)\ dx = 0 \ , \tag{8}$$

which was derived from the dispersion relation and the asymptotic behavior of the corresponding Compton amplitude. This sum rule is true at all Q^2 and does not follow from the OPE. It is rather a super-convergence relation based on Regge asymptotics as articulated in the review paper by Jaffe [22]. Many scenarios which could invalidate this sum rule have been discussed in the literature [23, 24, 2]. However, this sum rule was confirmed in perturbative QCD at order α_s with a $g_2(x,Q^2)$ structure function for a quark target [26]. Surprisingly a first precision measurement of g_2 by the E155 collaboration [20] at $Q^2 = 5$ GeV^2 but within a limited range of x has revealed a violation of this sum rule on the proton at the level of three standard deviations. In contrast, the neutron sum rule is poorly measured but consistent with zero at the one standard deviation. New high precision data on the neutron g_2 [25] at Q^2 below 1 GeV suggest that the BC sum rule is verified within errors.

2 Experimental status of $d_2^{n,p}(Q^2)$ and $\Gamma_2(Q^2)$ measurements

The early measurements of the g_2 spin structure function performed by the SMC [4] and E142 [5, 6] collaborations in the 90's were meant to reduce the systematic errors when extracting g_1 due to g_2's contribution in the measured parallel asymmetries. As the statistical precision of g_1 improved a better measurement of g_2 was required to minimize the error on g_1. E143 [7], E154 [8] and E155 [9] collaborations evaluated d_2 and published their results. However, until recently a few dedicated experiments, were performed to measure g_2 and extract ultimately d_2 with much improved statistical precision on the proton and the deuteron [20, 32] and ^{3}He [25, 28].

Fig. 3 shows d_2 of SLAC E155X [20] combined with the world data compared to several calculations. The proton result is generally consistent with the chiral quark model [33, 34] and some

bag models [35, 11, 17] while one to two standard deviations away from the QCD sum rule calculations [37, 38, 39]. The comparison with the lattice QCD calculation [15] is promising but the error bar on this calculation is still large. The Lattice Hadron Physics Collaboration based at Jefferson Lab has plans to calculate this matrix element for the proton and the neutron [27] and improve on the precision of the present lattice calculations.

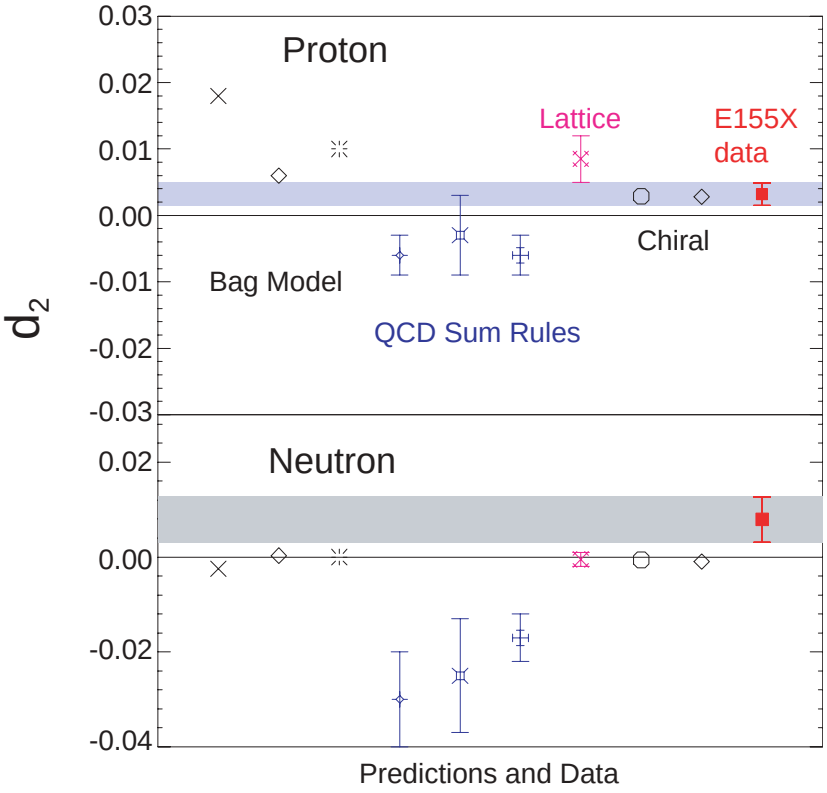

Figure 3: E155X results of the nucleon d_2 compared to several theoretical calculations (see text). Upper panel is for the proton and lower panel for the neutron.

For the neutron the situation is less clear since most models predict values consistent with a negative value or zero while the experimental result is positive and 2σ away from zero. In these models g_2^n is negative at large x therefore it is conceivable that the poor precision (Fig. 6) of the data in this region is affecting the overall sign of the result. It is important to note that from the point of view of a simple quark model, the d_2 matrix element of the neutron should be much smaller than that of the proton because of SU(6) spin-flavor symmetry. Therefore with the present precision of E155x neutron data it is difficult to draw any conclusions on the sign and size of the neutron higher twist (twist-three) contribution. Because d_2 is a second moment in x of the linear combination $(2g_1 + 3g_2)$ the neutron data set can be improved significantly at Jefferson Lab. Due to the x^2 weighting, the contribution of the small x region is supressed and thus using the the existing world data and future data in the region $x < 0.24$ should be sufficient to complete the integral. In fact the average Q^2 value of the world low x data is close to the value $Q^2 = 2$ GeV^2 of this proposal.

During JLab experiment E94-010 [25] which was aimed at measuring the Gerasimov-Drell-Hearn

extended sum, data on g_2 were taken using a polarized ^{3}He target across the resonance and deep inelatic region in the range $0.1 < Q^2 < 0.9$ GeV^2. New results on two moments of the neutron spin structure functions namely Γ_2^n and d_2^n are now available from this experiment. These results are shown in Fig. 4.

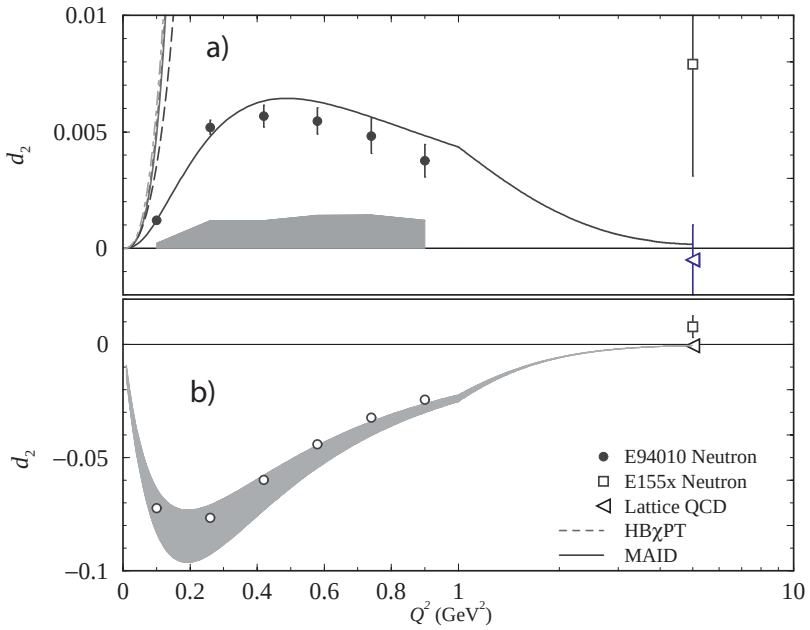

Figure 4: The quantity $d_2(Q^2)$ is shown at several values of Q^2 . The results of JLab E94-010 without the nucleon elastic contribution are the solid circles (top panel) . The grey band represents their corresponding systematic uncertainty. The SLAC E155 [20] neutron result shown if Fig. 3 is also shown here (open square). The solid line is the MAID calculation[40] while the dashed line is a HBχPT calculation[41] valid only at very low Q^2. The lattice prediction [15] at $Q^2 = 5$ GeV^2 for the neutron d_2 reduced matrix element is negative but close to zero. We note that all models shown in Fig. 3 predict a negative value or zero at large Q^2 where the elastic contribution is negligible. At moderate Q^2 the data show a positive d_2^n, and indicate a slow decrease with Q^2. The SLAC data also show a positive d_2^n value but with a rather large error bar. However, when the nucleon elastic contribution is added (bottom panel) the d_2^n quantity (open circles) is always negative and seems to approach the lattice result as Q^2 increases. The grey negative band represents the inelastic contribution from MAID added to a range of elastic contributions. Note the change of vertical scale.

In the investigation of higher twist contributions an important first step has already been taken with JLab experiment E97-103 [28], which will provide precision data of g_2^n in the deep inelastic region at low x ($0.17 < x < 0.21$) and will investigate its Q^2 evolution in the range $0.56 < Q^2 < 1.4$ (GeV^2) for a fixed value of $x \approx 0.2$. The unprecedented statistical accuracy expected in E97-103 allow us to probe the size of higher twists contributions by comparing directly the measured g_2^n to the leading twist contribution (twist-two contribution known as $g_2^{n(WW)}$ [30]). The experiment has been completed and the analysis is in its final stage. The preliminary results hint at a small but finite higher-twists contribution.

Two other approved experiments, JLab experiment E01-012 [31] which uses a polarized ^{3}He

target, and JLab experiment E01-006 [32] which uses polarized NH_3 and ND_3 targets, will add to the wealth of neutron spin structure functions data (g_1^n and g_2^n) in the resonance region. However, the first one emphasises the investigation of g_1 while the second provides data at $Q^2 = 1.3$ GeV^2 for g_2^p with high precision but limited precision for g_2^n.

The neutron result of g_2 extracted from the proton and deuteron measurements of E155X are shown in Fig. 6 along with what is expected from this proposal. The statistical accuracy already achieved in JLab E97-103 is shown for their highest Q^2 kinematics point, namely $Q^2 = 1.4$ GeV^2 and $x = 0.2$. We should point out that this proposed experiment is optimized to minimize the error on the determination of d_2^n not g_2^n. Obviously, time limitations would not allow us to provide for the statisticl precision at each x value for a direct comparison with models of g_2^n.

Finally, turning to the BC sum rule, the experimental situation is summarized in Fig. 5 where we show Γ_2^n measured in E94-010 (solid circles) and, including the elastic contribution (open circles) evaluated using a dipole form factor for G_M^n and the Galster fit for G_E^n. The positive light grey band corresponds to the total experimental systematic errors while the dark negative band in represents an estimated DIS contribution using g_2^{WW}. The solid line is the resonances contribution evaluated using MAID and the negative light-grey band is the neutron elastic contribution added to the measured data to determine Γ_2^n. The results are quite encouraging since the data show that the BC sum rule is verified within uncertainties over the Q^2 range measured. Our result is at odds with the reported violation of this sum rule on the proton at high Q^2 (where the elastic contribution is negligible) [20]. It is, however, consistent with the neutron result of SLAC E155 (open square) which unfortunately has a rather large error bar. In light of our results, a high statistical precision measurement in the range 1 GeV$^2 \leq Q^2 \leq 5$ GeV^2 would be of paramount importance for both the proton and neutron even if the x range is limited.

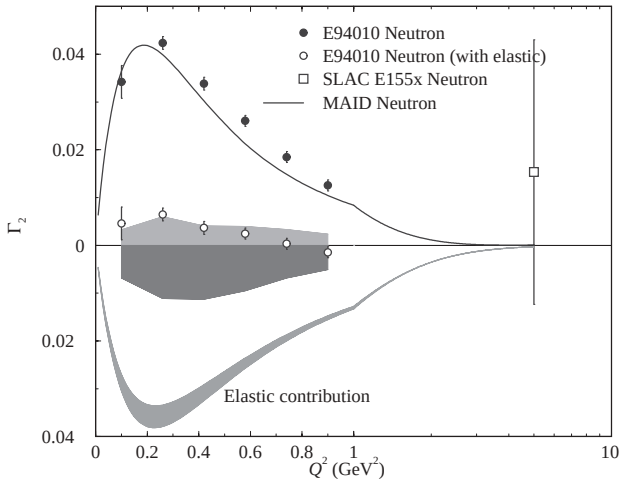

Figure 5: Results of Γ_2^n along with the average of the world data from DIS. The theoretical prediction for this quantity is zero (see text).

On the experimental side this situation can be improved using a target complementary to polarized deuterium (namely polarized ^{3}He) in order to extract the neutron information. JLab is in a unique position to provide high polarized luminosity to measure the large x region with good statistical precision. Unlike in previous experiments, world data fits of $R = \sigma_L/\sigma_T$, F_2 and g_1 will not be used to evaluate g_2, rather we shall measure absolute polarized cross sections for both

directions of the target spin, parallel and perpendicular and extract g_2 directly. Furthermore, in order to evaluate d_2 in those experiments, it is common practice to evolve the measured g_2 data from the measured Q^2 to a common Q^2 value, however, this evolution is not well understood for the twist-tree part of g_2. In contrast, our data will be measured at a constant Q^2.

We shall describe in this proposal how CEBAF is in a unique position to improve the neutron measurement of d_2^n by a factor of four and provide as well a reasonable test of the BC sum rule at $Q^2 = 2$ GeV^2.

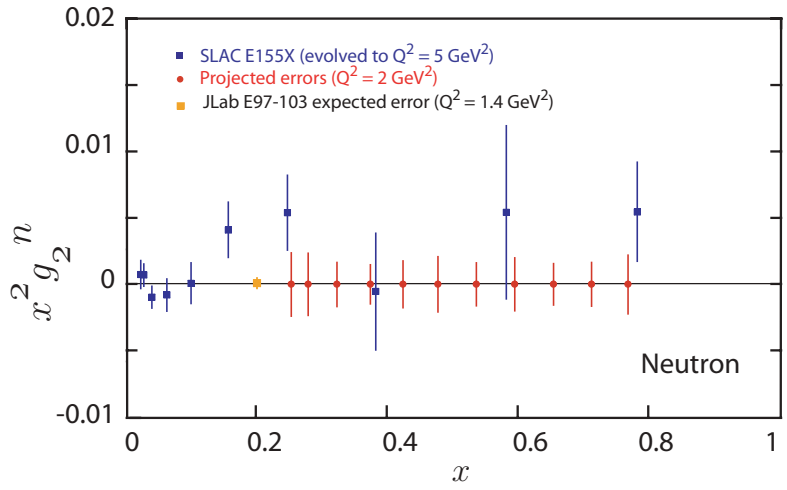

Figure 6: World average domiated by SLAC E155X results of the $x^2 g_2^n$ extracted by subtracting the proton from the deuteron following the prescription described in Ref.[29, 20]. Also shown are the statistical error achievable in this proposal on $x^2 g_2$ with a measurement rather optimized for determining d_2 with the best statistical precision.

3 Proposed Experiment

We propose to measure the unpolarized cross section $\sigma_0^{^3He}$, the parallel asymmetry $A_\parallel^{^3He}$ and perpendicular asymmetry $A_\perp^{^3He}$ at a constant Q^2. We will use the longitudinally polarized ($P_b = 0.8$) CEBAF electron beam and a 40-cm-long high pressure polarized ^{3}He target. The measurement will be performed at two incident electron beam energies E$_i$ = 5.7 GeV and 6.0 GeV using both HRS spectrometers at four scattering angles $\theta = 17.5°$, $20.0°$, $22.5°$ and $25.0°$. Five momentum settings for each spectrometer will cover the range $0.24 \leq x \leq 0.8$ at Q^2= 2.0 GeV^2. The target polarization orientation will be set longitudinal or transverse to the beam with a value of $P_t = 0.40$ while the beam helicity will be reversed at a rate of 30 Hz. A beam current of 15 μA combined with a target density of 2.5×10^{20} atoms/cm^3 provides a luminosity ranging between 5.9×10^{35} cm^{-2}s^{-1} and 8.3×10^{35} cm^{-2}s^{-1} depending on the effective target length at various angles.

3.1 Kinematics

The kinematic settings were chosen to allow a measurement at constant Q^2 over as wide an excitation energy range as possible. Fig. 7 shows in the (Q^2, x) plane the experimental excitation

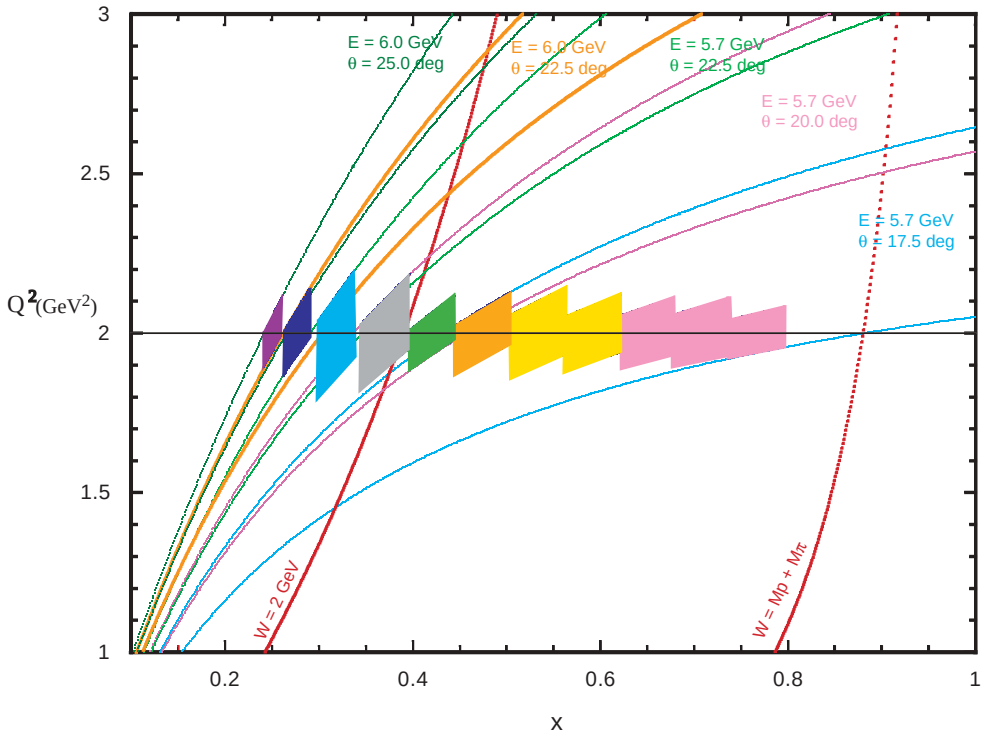

Figure 7: Proposed kinematic range for the measurement at a constant average Q^2 of 2 GeV^2. Each diamond represents the size of an (x,Q^2) bin chosen for this measurement. Each pair of common colored lines is plotted to indicate the possible range of (x,Q^2) due to the angular acceptance of the spectrometer for a fixed incident energy and scattering angle. The electron beam incident energy and the scattering angle and momentum of each spectrometer is chosen to keep the measured data at constant Q^2.

range we plan to cover from the pion threshold to the deep inelastic region including the nucleon resonance region. In order to keep Q^2 constant for each measured x bin, the scattering angle must range from 17.5° to 25°. Then by taking into account the angular acceptance of the HRS spectrometers ($\Delta\theta \approx \pm 25$ mrad) we find a continuous coverage of the x range at constant Q^2 (diamonds of different sizes shown on Fig. 7)

The main contribution to d_2 arises from the large x region because of the weighting of g_1 and g_2 by x^2 in the integration over x. The measurement of this region with high precision is important. In tables 3, 4 and 5 we have listed the kinematical conditions for each spectrometer needed to cover the proposed x region.

3.2 The Polarized Beam

In this proposal we shall assume, that the achievable beam polarization at CEBAF is 80% with a current of 15μA. While about 70% electron beam polarization has been delivered on a regular basis to E94-010 and E95-001 we are optimistic that by the time this experiment runs and with the experience gained using the strained GaAs cathodes, 80% beam polarization will be achieved. The polarization of the beam will be measured with the Hall A Moller and Compton polarimeters.

3.3 The Polarized ^{3}He Target

The polarized target will be based on the principle of spin exchange between optically pumped alkali-metal vapor and noble-gas nuclei [42, 43, 44]. It is the same as that used in JLab experiments E94-010, E95-001, E97-103 and E99-117 in Hall A.

A central feature of the target will be sealed glass target cells, which under operating conditions, will contain a ^{3}He pressure of about 10 atmospheres. As indicated in Fig. 8, the cells will have two chambers, an upper chamber in which the spin exchange takes place, and a lower chamber, through which the electron beam will pass. In order to maintain the appropriate number density of the alkali-metal Rubidium the upper chamber will be kept at a temperature of 170–200° using an oven constructed of high temperature plastic Torlon. The density of the target will be about 2.5×10^{20} atoms/cm^3. The lower cell length will be 40 cm such that the end glass windows are not seen by the spectrometer acceptance when it is set at a scattering angle of 17.5° and larger. The effective target thickness will range from 6.0×10^{21} atoms/cm^2 to 8.3×10^{21} atoms/cm^2, since the spectrometer acceptance sees a length of 7 cm/$\sin\theta_e$

The main components of the target are shown in Fig. 8. The main "coils" shown are large Helmholtz coils used to apply a static magnetic field of about 25 Gauss. Also shown are the components for the NMR and EPR polarimetry. The NMR components of the target include a set of RF drive coils, and a separate set of pickup coils. Not shown in the figure are the NMR electronics, which include an RF amplifier, a lock-in amplifier, some bridge circuitry, and the capability to sweep the static magnetic field. The EPR components include an EPR excitation coil and a photodiode for detection of the EPR line. The oven shown in Fig. 8 is heated with forced hot air. The optics system include a system of 4 diode lasers for longitudinal pumping and 4 for transverse pumping. A polarizing beam splitter, lens system and a quarter wave plate are required to condition each laser beam line and provide circular polarization.

3.3.1 Operating Principles

The time evolution of the ^{3}He polarization can be calculated from a simple analysis of spin-exchange and ^{3}He nuclear relaxation rates[45]. Assuming the ^{3}He polarization $\mathrm{P_{^3He}} = 0$ at $t = 0$,

$$\mathrm{P_{^3He}(t)} = \mathrm{P_{Rb}} \left(\frac{\gamma_{\mathrm{SE}}}{\gamma_{\mathrm{SE}} + \Gamma_{\mathrm{R}}}\right) \left(1 - \mathrm{e}^{-(\gamma_{\mathrm{SE}}+\Gamma_{\mathrm{R}})\,\mathrm{t}}\right) \tag{9}$$

where γ_{SE} is the spin-exchange rate per ^{3}He atom between the Rb and ^{3}He, Γ_{R} is the relaxation rate of the ^{3}He nuclear polarization through all channels other than spin exchange with Rb, and $\mathrm{P_{Rb}}$ is the average polarization of the Rb atoms. Likewise, if the optical pumping is turned off at $t = 0$ with $\mathrm{P_{^3He}} = \mathrm{P_0}$, the ^{3}He nuclear polarization will decay according to

$$\mathrm{P_{^3He}(t)} = \mathrm{P_0}\,\mathrm{e}^{-(\gamma_{\mathrm{SE}}+\Gamma_{\mathrm{R}})\,\mathrm{t}}. \tag{10}$$

The spin exchange rate γ_{SE} is defined by

$$\gamma_{\mathrm{SE}} \equiv \langle \sigma_{\mathrm{SE}}\, v \rangle\, [\mathrm{Rb}]_{\mathrm{A}} \tag{11}$$

where, $\langle \sigma_{\mathrm{SE}}\, v \rangle = 1.2 \times 10^{-19}$ cm^3/sec is the velocity-averaged spin-exchange cross section for Rb–^{3}He collisions[45, 46, 47] and $[\mathrm{Rb}]_{\mathrm{A}}$ is the average Rb number density seen by a ^{3}He atom. The target operates with $1/\gamma_{\mathrm{SE}} = 8$ hours. From equation (9) it is clear that the best possible ^{3}He polarization is obtained by maximizing γ_{SE} and minimizing Γ_{R}. But from equation (11) we can see that maximizing γ_{SE} means increasing the alkali-metal number density, which in turn means more

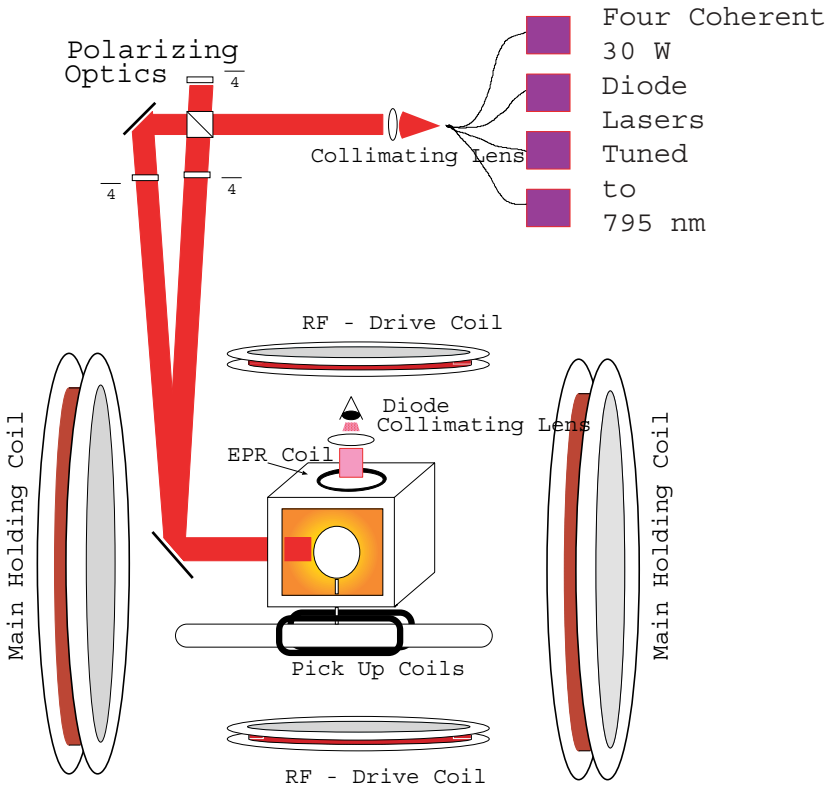

Figure 8: JLab Hall A polarized ^{3}He target setup.

laser power. The number of photons needed per second must compensate for the spin relaxation of Rb spins. In order to achieve $1/\gamma_{\rm SE} = 8$ hours, about 50 Watts of usable laser light at a wavelength of 795 nm will be required.

The rate at which polarization is lost is characterized by Γ and has four principle contributions. An average electron beam current of about 15 μA will result in a depolarization rate of $\Gamma_{beam} = 1/30$ hours [48]. The cells produced in previous experiments typically have an intrinsic rate of $\Gamma_{cell} = 1/50$ hours. This has two contributions, relaxation that occurs during collisions of ^{3}He atoms due to dipole-dipole interactions, and relaxation that is largely due to the interaction of the ^{3}He atoms with the walls. Finally, relaxation due to magnetic field inhomogeneities was held to about $\Gamma_{\nabla B} = 1/100$ hours. Collectively, under operating conditions, we would thus expect

$$\Gamma_R = \Gamma_{beam} + \Gamma_{cell} + \Gamma_{\nabla B} = 1/30\,\text{hours} + 1/50\,\text{hours} + 1/100\,\text{hours} = 1/16\,\text{hours}.$$

Thus, according to equation (9), the target polarization cannot be expected to exceed

$$P_{max} = \frac{\gamma_{\rm SE}}{\gamma_{\rm SE} + \Gamma_{\rm R}} = 0.66$$

Realistically, a Rb polarization of 100% in the pumping chamber will not be achieved, which will reduce the polarization to about 40%.

During E94-010 and E95-001 we achieved a polarization of about 30-35% when a beam current of 15μA was used. The beam depolarization was slightly larger than expected and this was the

first time that such a large beam current was used for an extended period time. An R&D effort is underway by JLab and the polarized ^{3}He target collaboration to improve the achievable polarization under the beam conditions proposed in this experiment.

3.3.2 Target Cells

The length of the cell has been chosen to be 40 cm so that the end windows are not within the acceptance of the Hall A spectrometers at angles equal to 17.5° and larger. The end windows themselves will be about 100 μm thick.

3.3.3 The Optics System

As mentioned above, approximately 50 W of "usable" light at 795 nm will be required. By "usable", we mean circularly polarized light that can be readily absorbed by the Rb. It should be noted that the absorption line of Rb has a full width of several hundred GHz at the high pressures of ^{3}He at which we will operate. Furthermore, since we will operate with very high Rb number densities that are optically quite thick, even light that is not well within their absorption line width can still be absorbed.

The laser system is similar to that used in E94-010. It consists of commercially available 30 Watt fiber-coupled diode laser systems (from COHERENT INC.). Four such lasers are used to pump along the transverse direction and three along the longitudinal direction. The efficiency of these lasers has been tested during experiment E94-010 and E95-001 and found to be totally adequate for this experiment's needs.

3.3.4 Polarimetry

Polarimetry is accomplished by two means. During the experiment, polarization is monitored using the NMR technique of adiabatic fast passage (AFP)[49]. The signals are calibrated by comparing the ^{3}He NMR signals with those of water. The calibration is then independently verified by studying the frequency shifts that the polarized ^{3}He nuclei cause on the electron paramagnetic resonance (EPR) lines of Rb atoms [48]. Both methods were used in E94-010 and we found as expected that the NMR measurements with water calibration are consistent with the EPR results.

3.4 The Spectrometers Setup

We plan to use both HRS spectrometers in Hall A. We will use the right spectrometer with its standard detector package for electrons and the left spectrometer with an added double layer lead glass calorimeter which was first used in E94-010. Each spectrometer will then consist of;

- Two vertical Drift Chambers (VDCs) for the measurement of momentum and production angle.
- Gas Čerenkov counter for pion rejection.
- A set of scintillators for triggering on charged particles.
- A double layer lead glass calorimeter for additional pion rejection.

As the E94-010 analysis shows, the pion rejection factor with the Čerenkov counter and the lead glass calorimeter are better than 2×10^{-4} which is sufficient for our worst case.

Because the maximum momentum attainable by each spectrometer is different (4.30 GeV for the HRS-l and 3.17 GeV for the HRS-r) we have assigned HRS-l to perform the measurements for electron momenta greater than 3 GeV and HRS-r for those measurements with momenta equal or less than 3 GeV. We optimized the time sharing between the two spectrometers (see Table 4 and 5). Although we need to make few spectrometer angle changes to keep our measurement at constant Q^2. Specific advantages make these spectrometers a well matched tool for the proposed measurement.

- Good electron events in the spectrometer are in principle due only to electron scattering off ^{3}He nuclei since the target cell glass windows are outside the spectrometer acceptance. However, excellent target reconstruction by the HRS spectrometers allows for better background rejection.

- An excellent resolution of the spectrometers permits the measurement of elastic scattering off ^{3}He needed for an absolute calibration of the detector in order to measure absolute cross sections.

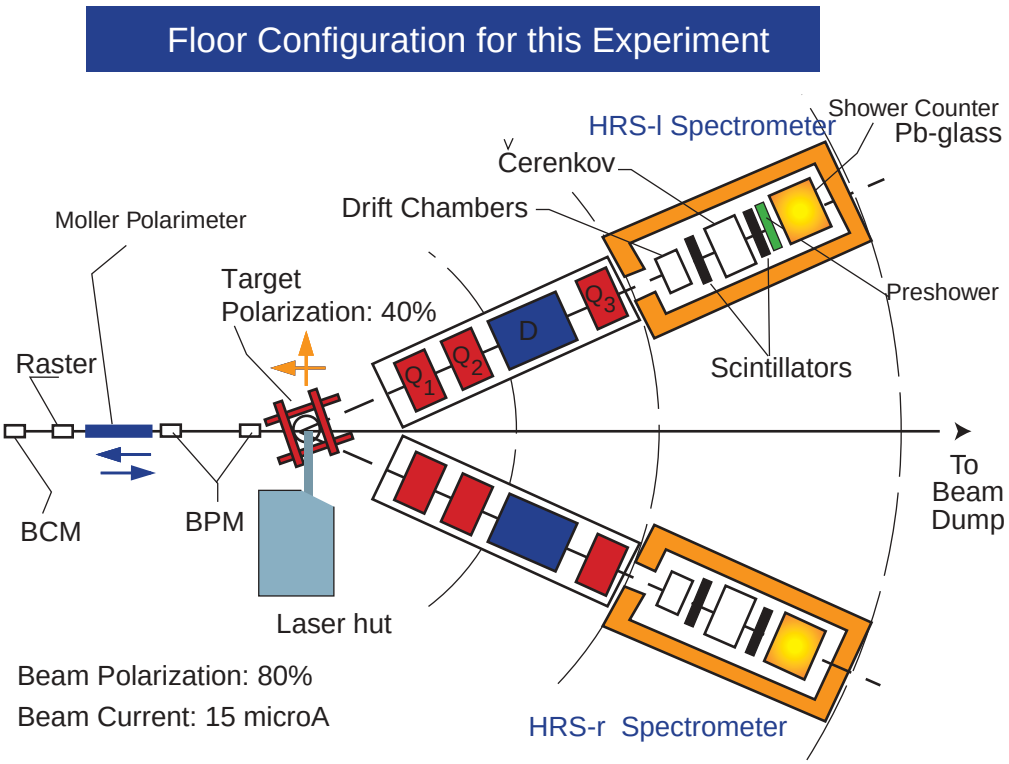

Figure 9: JLab Hall A floor setup using the HRS spectrometers and the polarized 3He target. Note that their maximum central momentum reach is not the same. It is 4.3 GeV for the left HRS and 3.17 GeV for right HRS

4 Evaluation of d_2^n

The goal of this experiment is to obtain the d_2 from a direct measurement of the unpolarized cross section σ_0 and the parallel $A_\parallel$ and perpendicular $A_\perp$ asymmetries on ^{3}He. Equivalently d_2 is obtained from the measurement of the linear combination of the spin structure functions $g_1(x,Q^2)$ and $g_2(x,Q^2)$ and forming the second moment of this combination namely,

$$d_2(Q^2) = \int_0^1 x^2[2g_1(x,Q^2) + 3g_2(x,Q^2)]\ dx = \int_0^1 \tilde{d}_2(x,Q^2)\ dx \tag{12}$$

The spin structure functions can be expressed in terms of asymmetries and unpolarized cross sections as follow;

$$g_1 = \frac{MQ^2}{4\alpha^2}\frac{y}{(1-y)(2-y)}2\sigma_0\left[A_\parallel + \tan\frac{\theta}{2}A_\perp\right] \tag{13}$$

$$g_2 = \frac{MQ^2}{4\alpha^2}\frac{y^2}{2(1-y)(2-y)}2\sigma_0\left[-A_\parallel + \frac{1+(1-y)\cos\theta}{(1-y)\sin\theta}A_\perp\right] \tag{14}$$

where σ_0 is the unpolarized cross section, Q^2 is the four momentum transfer, α the electromagnetic coupling constant, θ the scattering angle and $y = (E-E')/E$ the fraction of energy transferred to the target. $A_\parallel$ and $A_\perp$ are the parallel and perpendicular asymmetries,

$$A_\parallel = \frac{\sigma^{\downarrow\Uparrow} - \sigma^{\uparrow\Uparrow}}{2\sigma_0}, \qquad A_\perp = \frac{\sigma^{\downarrow\Rightarrow} - \sigma^{\uparrow\Rightarrow}}{2\sigma_0} \tag{15}$$

From (12), (13) and (14) we can express the integrand of d_2 directly in terms of measured asymmetries and unpolarized cross section as follows:

$$\tilde{d}_2(x,Q^2) = x^2[2g_1(x,Q^2) + 3g_2(x,Q^2)] \tag{16}$$

$$= \frac{MQ^2}{4\alpha^2}\frac{x^2y^2}{(1-y)(2-y)}\sigma_0\left[\left(3\frac{1+(1-y)\cos\theta}{(1-y)\sin\theta} + \frac{4}{y}\tan\frac{\theta}{2}\right)A_\perp + \left(\frac{4}{y} - 3\right)A_\parallel\right] \tag{17}$$

The above expression of the integrand is used for the following purposes:

- Determination of the time sharing between the transverse and the longitudinal measurement to minimize the statistical error on d_2 not on g_2 as in previous experiments.
- Determination of the effect of the target polarization orientation misalignment on the systematic error of d_2
- Determination of the systematic error on d_2 due to the systematic errors of the cross section and asymmetries measurements.

The measurement consists of collecting data at two incident energies ($E_i = 5.7$ GeV and 6.0 GeV) and four scattering scattering angles ($\theta = 17.5^\circ, 20.0^\circ, 22.5^\circ$ and 25.0°) and for eight spectrometer momentum settings to cover the range $0.25 \le x \le 0.8$. The measured raw ^{3}He counting parallel asymmetry $\Delta_\parallel$ and perpendicular asymmetry $\Delta_\perp$ are converted to the experimental asymmetries $A_\parallel^{^3He}$, and $A_\perp^{^3He}$ respectively, using the relation

$$A_\perp^{^3He} = \frac{\Delta_\perp}{P_b P_t \cos\phi} \qquad A_\parallel^{^3He} = \frac{\Delta_\parallel}{P_b P_t} \tag{18}$$

$$\Delta_\perp = \frac{(N^{\uparrow\Rightarrow} - N^{\uparrow\Rightarrow})}{(N^{\uparrow\Rightarrow} + N^{\uparrow\Rightarrow})} \qquad \Delta_\parallel = \frac{(N^{\downarrow\Uparrow} - N^{\uparrow\Uparrow})}{(N^{\downarrow\Uparrow} + N^{\uparrow\Uparrow})} \tag{19}$$

where $N^{\uparrow\Downarrow}$ ($N^{\uparrow\Uparrow}$) and $N^{\uparrow\Rightarrow}$ ($N^{\uparrow\Rightarrow}$) represent the rate of scattered electrons for each bin in x and Q^2 when the electron beam helicity and target spin are parallel or perpendicular. ϕ is the angle between the scattering plane and the plane formed by the incoming beam and the perpendicular target polarization. $P_b = 0.80$ and $P_t = 0.40$ are the beam and target polarization respectively. The target length (40 cm) is chosen such that no extra dilution of the asymmetry occurs from unpolarized scattering off the glass windows. However, empty target measurements will be performed to insure that no spurious unpolarized background originating in the target area reduces the measured physics asymmetries. The kinematics and electron rates are presented in Table 3. We used the Whitlow 1990 [50] parametrization of unpolarized structure functions from measurements of deep inelastic scattering on the proton and the deuteron. We added incoherently the appropriate structure functions to generate the ^{3}He cross sections. The rates were determined assuming a solid angle evaluated from the bins shown in Fig. 7 and a luminosity varying from 6.0×10^{35} cm^{-2}s^{-1} to 8.0×10^{35} cm^{-2}s^{-1}. The times for the transverse and longitudinal measurements were determined by optimizing the time sharing for the best precision on the integrand $\tilde{d}_2$. If we set

$$\alpha = \frac{MQ^2}{4\alpha^2}\frac{x^2y^2}{(1-y)(2-y)}\sigma_0\left(3\frac{1+(1-y)\cos\theta}{(1-y)\sin\theta}+\frac{4}{y}\tan\frac{\theta}{2}\right) \quad (20)$$

$$\beta = \frac{MQ^2}{4\alpha^2}\frac{x^2y^2}{(1-y)(2-y)}\sigma_0\left(\frac{4}{y}-3\right) \quad (21)$$

The optimum ratio between the parallel and perpendicular counts is

$$N_\parallel = \frac{\beta}{\alpha}N_\perp \quad (22)$$

The total number of counts $N_\perp$ is given by

$$N_\perp = \frac{\alpha(\alpha+\beta)}{P_b^2P_t^2f^2(\Delta\tilde{d}_2)^2} \quad (23)$$

$f = W_1^n/W_1^{^3He}$ is the fraction of scattering originating from the neutron compared to ^{3}He. We required an absolute statistical uncertainty on the integrand $\Delta\tilde{d}_2^n$ between $7.5\times\ 10^{-3}$ and $5\times\ 10^{-3}$ at different x bins. This in turn leads to an absolute statistical precision on d_2^n of $\Delta d_2^n \approx 1.18\times10^{-3}$. This value is to be compared with $\Delta d_2^n \approx 5\times10^{-3}$ of SLAC E155X.

The pion background was estimated using the EPC program [51] which was normalized against measurements carried at JLab in a similar kinematic range. The results of the estimate are listed in Table 1 were the π/e^- ratio ranges from a negligible value in the highest x bin to a value of about twenty in the lowest x bin. Given the pion rejection performance of the combination Čerenkov and lead glass calorimeter, we should be able to keep this correction at a negligible level. Furthermore, we shall also measure the pion asymmetry using the hadron spectrometer in the lowest three x bins.

The radiative corrections (RC) will be performed in two stages. First the internal corrections will be evaluated following the procedure developed by Bardin and Shumeiko[52] for the unpolarized case and extended to the spin dependent lepto-production cross sections by Akushevish and Shumeiko[53, 54]. Second, using these internally corrected cross sections, the external corrections (for thick targets) are applied by extending the procedure developed for the unpolarized cross sections by Tsai[55, 56] with modifications appropriate for this experiment.

To evaluate the experimental systematic uncertainty of d_2^n we used relative uncertainties in the cross sections and asymmetries achieved in E94-010. Table 4 summarizes these uncertainties. One item of concern was the effect of the target relative spin misalignment between the transverse and

Table 1: π^-/e^- each x bin planned in this measurement

E_i (GeV)	θ_e °	E' (GeV)	x	W (GeV)	dσ^{π^-} (nb/GeV/sr)	π^- rate (Hz)	π^-/e^-
5.70	16.40	4.310	0.766	1.22	0.51	0.03	0.006
5.70	16.63	4.197	0.710	1.30	0.94	0.09	0.013
5.70	16.90	4.064	0.652	1.40	1.68	0.20	0.024
5.70	17.24	3.903	0.593	1.50	2.98	0.48	0.030
5.70	17.70	3.705	0.534	1.62	5.40	1.31	0.062
5.70	18.33	3.458	0.475	1.76	10.4	2.67	0.118
5.70	19.14	3.173	0.422	1.90	20.8	5.01	0.264
5.70	20.27	2.833	0.372	2.06	44.7	28.54	0.673
5.70	22.16	2.375	0.321	2.26	120.3	92.13	2.41
6.00	22.70	2.152	0.277	2.47	253.3	141.25	6.04
6.00	25.14	1.760	0.251	2.62	574.9	245.44	18.7

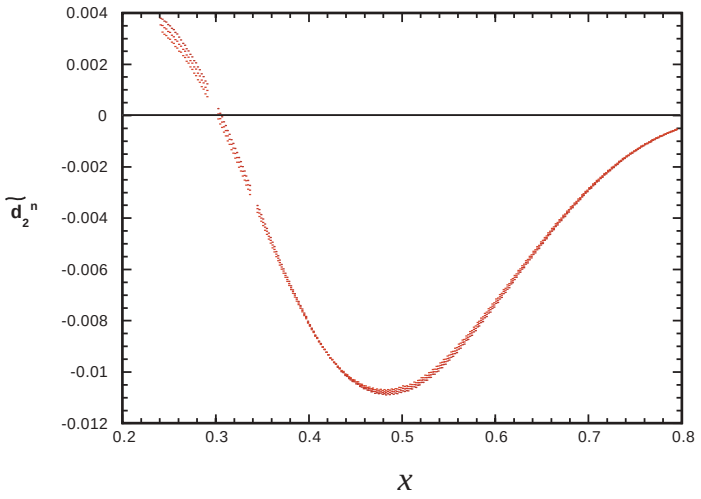

Figure 10: Effect of target relative spin misalignment by 0.5° between the transverse and longitudinal measurements

longitudinal direction measurements. Fig. 10 shows this effect at each value of x on the integrand of d_2. A relative error of 0.5° in the relative direction of the transverse versus perpendicular results in a relative error $\Delta d_2/d_2 = 0.15\%$. Using the Weigel *et al.* [33] model of g_2 and g_1 we estimated $\Delta d_2/d_2$ to be of the order of 10 % and thus an absolute systematic uncertainty of about 10^{-3}. We believe we can achieve a relative error of 0.2° in the target spin alignment.

Even with our improved projected statistical precision the total uncertainty in d_2^n is still dominated by the statistical accuracy of the measurement not its systematic.

An elastic scattering asymmetry measurement is planned at low energy ($E_i = 1.0$ GeV $\theta = 17.5°$) in order to calibrate our spin dependent absolute cross sections. This quantity can be evaluated

Table 2: List of the systematic error contributions to d_2^n

Item description	Subitem description	Relative uncertainty
Target polarization		4 %
Beam polarization		3 %
Asymmetry (raw)		
	• Target spin direction (0.5°)	$\approx 1.5 \times 10^{-3}$
	• Beam charge asymmetry	200 ppm
Cross section (raw)		
	• PID efficiency	$\approx$ 1 %
	• Background Rejection efficiency	$\approx$ 1 %
	• Beam charge	$<$ 1 %
	• Beam position	$<$ 1 %
	• Acceptance cut	2-3 %
	• Target density	2-3 %
	• Nitrogen dilution	2-3 %
	• Dead time	<1 %
	• Finite Acceptance cut	<1%
Radiative corrections		$\leq$ 10 %
From ^{3}He to Neutron correction		5 %
Total effect		$\leq$ 10 %
Estimate of contributions	$\int_{0.003}^{0.241} \tilde{d}_2^n \, dx$	4.8×10^{-4}
from unmeasured regions	$\int_{0.767}^{0.999} \tilde{d}_2^n \, dx$	3.9×10^{-5}
Projected absolute statistical uncertainty		$\Delta d_2 \approx 1.18 \times 10^{-3}$
Projected absolute systematic uncertainty assuming $d_2 = 5 \times 10^{-3}$		$\Delta d_2 \approx 5 \times 10^{-4}$

Table 3: Parameters per bin in (Q^2,x) plane for the proposed experiment

E_i (GeV)	bin central p (GeV)	x	Δx	Q^2 (GeV^2)	W (GeV)	Rate (Hz)	Time$_\perp$ hours	Time$_\parallel$ hours
5.700	4.31	.766	.580E-01	2.00	1.22	5.03	157.	79.1
5.700	4.20	.710	.580E-01	2.00	1.30	6.85		
5.700	4.06	.652	.570E-01	2.00	1.40	8.23		
5.700	3.90	.593	.590E-01	2.00	1.50	16.0	122.	43.9
5.700	3.71	.534	.590E-01	2.00	1.62	21.1		
5.700	3.46	.475	.590E-01	2.00	1.76	22.6	88.0	23.9
5.700	3.17	.422	.480E-01	2.00	1.90	19.0	151.	34.2
5.700	2.83	.372	.520E-01	2.00	2.06	42.4	99.3	18.2
5.700	2.38	.321	.340E-01	2.00	2.26	38.1	83.2	11.5
6.000	2.15	.277	.270E-01	2.00	2.47	23.4	70.8	7.61
6.000	1.76	.251	.180E-01	2.00	2.61	13.1	121.	10.2

using the measured electric and magnetic form factors of ^{3}He. This measurement would actually determine the polarization of the ^{3}He nuclei along the electron beam path. False asymmetries will be checked to be consistent with zero by comparing data with target spins in opposite directions.

Also contributing to the dilution of the asymmetry is the pair-electron contamination. This correction is x dependent, and is relevant only in the lowest x region. This contamination was estimated to be no more than 6% in the worst case and will be measured in this experiment by reversing the spectrometer polarity on the right arm spectrometer.

The spectrometers cannot be used in a symmetric configuration when taking data since they don't access the same maximum range of momentum. For this reason the low x data will be taken mainly using the HRS-r spectrometer and most of the large x data will be acquired using the HRS-l spectrometer. Tables 4 and 5 show the kinematics and time for each spectrometer acquiring data. The right spectrometer will also be used to measure the positron contamination at the lowest x bins, while the HRS-l completes its measurements at large x. We will use the HRS-l for 619 hours with beam on target to complete this measurement.

Table 4: Sequence of measurements carried by the HRS-l spectrometer

E_i GeV	θ deg	HRS-l Central p GeV		$\text{Time}_\perp$ hours	$\text{Time}_\parallel$ hours
6.0	22.5	2.167		35.4	3.8
6.0	25.0	1.756		60.5	5.1
5.7	17.5	4.069		157	79.1
5.7	17.5	3.794		122	43.9
5.7	17.5	3.538		88	23.9
			Total	462.9	155.8

Table 5: Sequence of measurements carried by the HRS-r spectrometer

E_i GeV	θ deg	HRS-r Central p GeV		$\text{Time}_\perp$ hours	$\text{Time}_\parallel$ hours
6.0	22.5	2.167		35.4	3.8
6.0	25.0	1.756		60.5	5.1
5.7	20.0	3.075		151.	34.2
5.7	20.0	2.867		99.3	18.2
5.7	22.5	2.324		83.2	11.5
			Total	429.4	72.8

5 Spin Structure Functions: From ^{3}He to the Neutron

For spin-dependent structure, because the deuteron polarization is shared roughly equally between the proton and neutron, extraction of neutron spin structure functions requires a precise knowledge of the proton spin structure, in addition to the nuclear effects [57]. This problem is compounded by the fact that the spin-dependent structure functions of the proton are typically much larger than those of the neutron, making extraction of the latter especially sensitive to small uncertainties in the proton structure functions. On the other hand, since the neutron in ^{3}He carries almost 90% of the nuclear spin, polarized ^{3}He is an ideal source of polarized neutrons.

The three-nucleon system has been studied for many years, and modern three-body wave functions have been tested against a large array of observables which put rather strong constraints on the nuclear models [58]. In particular, over the past decade considerable experience has been acquired in the application of three-body wave functions to deep-inelastic scattering [59, 60, 61].

The conventional approach employed in calculating nuclear structure functions in the region $0.3 < x < 0.8$ is the impulse approximation, in which the virtual photon scatters incoherently from individual nucleons in the nucleus [62]. Corrections due to multiple scattering, NN correlations or multi-quark effects are usually confined to either the small-x ($x < 0.2$), or very large-x ($x > 0.9$) regions. In the impulse approximation the g_1 structure function of ^{3}He, in the Bjorken limit ($Q^2, \nu \to \infty$), is obtained by folding the nucleon structure function with the nucleon momentum distribution in ^{3}He, Δf_N:

$$g_1^{^3\mathrm{He}}(x) \;=\; \int_x^3 \frac{dy}{y}\; \{2\Delta f_p(y)\; g_1^p(x/y) \;+ \Delta f_n(y)\; g_1^n(x/y)\}\,, \tag{24}$$

where y is the fraction of the ^{3}He momentum carried by the nucleon, and the dependence on scale, Q^2, has been suppressed. The nucleon momentum distributions $\Delta f_N(y)$ are calculated from the three-body nuclear wave function, which are obtained by either solving the Faddeev equation [63] or using variational methods [60], and are normalized such that:

$$\int_0^3 dy\; \Delta f_N(y) \;=\; \rho_N\;, \tag{25}$$

where ρ_N is the polarization of the nucleon in ^{3}He. While the full three-body wave function involves summing over many channels, in practice the three lowest states, namely the S, S' and D, account for over 99% of the normalization. Typically, one finds $\rho_n \approx 87\%$ and $\rho_p \approx -2\%$ [58, 59, 60, 61, 63].

The smearing in Eq.(24) incorporates the effects of Fermi motion and nuclear binding. Correctly accounting for these effects is important when attempting to extract information on nucleon structure functions from nuclear data at $x > 0.6$, as well as for determining higher moments of structure functions, in which the large-x region is more strongly weighted.

The nuclear corrections to the g_2^n structure function can be evaluated analogously to those for g_1^n.

One can estimate the order of magnitude of the possible effects by considering the twist-2 part of g_2^n, which is determined from g_1^n through the Wandzura-Wilczek relation [30] [66]:

$$g_2^{^3\mathrm{He}}(x)\Big|_{\mathrm{tw-2}} \;=\; -g_1^{^3\mathrm{He}}(x) \;+\; \int_x^3 \frac{dy}{y}\; g_1^{^3\mathrm{He}}(x/y)\;, \tag{26}$$

where $g_1^{^3\mathrm{He}}$ is given by Eq.(24).

Since the main objective of the experiment is to extract the second moment of $3g_2^n + 2g_1^n$, namely $\int dx\; x^2(3g_2^n(x) + 2g_1^n(x))$, the sensitivity of the correction to x variations of the integrand is reduced compared to a direct extraction of the g_2 or g_1.

The difference in the second moments of $g_2^{^3\mathrm{He}}$ between the smearing and no-smearing cases, is at the level of a few percent, as is the difference between the convolution results using different ^{3}He wave functions.

While the nuclear model dependence of the nuclear correction appears to be relatively weak for the twist-2 approximation in the Bjorken limit, an important question for the kinematics relevant to this experiment is how are these effects likely to be modified at finite Q^2? To address this question one needs to obtain generalizations of Eqs. (24) and (26) which are valid at any Q^2, and also for the twist-3 component of g_2. In fact, at finite Q^2 one finds contributions from g_1^n to $g_2^{^3\mathrm{He}}$, and from g_2^N to $g_1^{^3\mathrm{He}}$. The latter vanish in the Bjorken limit, but the former are finite, although they depend on the Fermi momentum of the bound nucleons. To estimate these corrections one needs to work directly in terms of the (unintegrated) spectral function $S(\vec{p},E)$, where p is the bound nucleon momentum and E the separation energy, rather than the momentum distribution functions $\Delta f_N(y)$. Following Schulze & Sauer [61], it is convenient to parameterize the ^{3}He spectral function according to:

$$S(\vec{p},E) \;=\; \frac{1}{2}\left(f_0 + f_1 \vec{\sigma}_N\cdot\vec{\sigma}_A + f_2\left[\vec{\sigma}_N\cdot\hat{p}\;\vec{\sigma}_A\cdot\hat{p}\;-\frac{1}{3}\vec{\sigma}_N\cdot\vec{\sigma}_A\right]\right)\;, \tag{27}$$

where $\vec{\sigma}_N$ and $\vec{\sigma}_A$ are the spin operators of the nucleon and ^{3}He, respectively, and the functions $f_{0,1,2}$ are scalar functions of $|\vec{p}|$ and E. The function f_0 contributes to unpolarized scattering, while f_1 and f_2 determine the spin-dependent structure functions. In terms of these functions, at finite Q^2 one has a set of coupled equations for $g_1^{^3\mathrm{He}}$ and $g_2^{^3\mathrm{He}}$ [68]:

$$\begin{aligned} & x\left(g_1^{^3\mathrm{He}}(x,Q^2) + (1-\gamma^2)g_2^{^3\mathrm{He}}(x,Q^2)\right) \\ = & \sum_{N=p,n}\int d^3p\; dE\;(1-\frac{\epsilon}{M})\left\{\left[\left(1+\frac{\gamma p_z}{M}+\frac{p_z^2}{M^2}\right)f_1 + \left(-\frac{1}{3}+\hat{p}_z^2+\frac{2\gamma p_z}{3M}+\frac{2p_z^2}{3M^2}\right)f_2\right]\; z g_1^N(z,Q^2)\right. \\ & \left. + (1-\gamma^2)(1+\frac{\epsilon}{M}\left[f_1+\left(\frac{p_z^2}{\vec{p}^2}-\frac{1}{3}\right)f_2\right]\frac{z^2}{x}g_2^N(z,Q^2)\right\}\;, \end{aligned} \tag{28}$$

$$\begin{aligned} & x\left(g_1^{^3\mathrm{He}}(x,Q^2) + g_2^{^3\mathrm{He}}(x,Q^2)\right) \\ = & \sum_{N=p,n}\int d^3p\; dE\;(1-\frac{\epsilon}{M})\left\{\left[\left(1+\frac{p_x^2}{M^2}\right)f_1 + \left(\vec{p}_x^{\,2}-\frac{1}{3}+\frac{2p_x^2}{3M^2}\right)f_2\right] z g_1^N(z,Q^2)\right. \\ & \left. + \left[\left(1+\frac{p_x^2}{M^2}(1-z/x)\right)f_1 + \left(\vec{p}_x^{\,2}-\frac{1}{3}+\frac{2p_x^2}{3M^2}(1-z/x)-\frac{\gamma p_z\hat{p}_x^2}{M}\frac{z}{x}\right)f_2\right] z g_2^N(z,Q^2)\right\}\;, \end{aligned} \tag{29}$$

with $\gamma = \sqrt{1+4M^2x^2/Q^2}$ a kinematical factor parameterizing the finite Q^2 correction, $\epsilon \equiv \vec{p}^2/4M - E$, and $z = x/(1+(\epsilon+\gamma p_z)/M)$. Equations. (28) and (29) can then be solved to obtain $g_1^{^3\mathrm{He}}$ and $g_2^{^3\mathrm{He}}$ explicitly. The nuclear correction of most interest for this experiment is that to the g_2 structure function.

To quantify the size of the kinematical Q^2 dependence, as distinct from the Q^2 dependence in the nucleon structure function itself, we use the same input neutron structure function for all values of Q^2 at which $xg_2^{^3\mathrm{He}}$ is evaluated. We find that the effect of the kinematical Q^2 dependence is rather small at $Q^2 \sim 1$–2 GeV^2, and only becomes noticable for low $Q^2 \sim 0.2$ GeV^2. Furthermore, we find that at these values of Q^2 the g_1^n contribution to $g_2^{^3\mathrm{He}}$ is negligible compared with the lowest order neutron polarization correction. This confirms earlier analyses of the nuclear corrections [69]

There was also an investigation into the role of the $\Delta(1232)$ in deep-inelastic scattering on polarized ^{3}He and its effects on the g_1 neutron spin structure function extraction [67]. The authors

estimated that when taking the effect of the Δ into account the values of the first moment of g_1^n increases by $6 \div 8$ %.

In summary, all of the nuclear structure function analyses that have been performed suggest that both the neutron g_1^n and g_2^n deep-inelastic structure functions can be extracted from ^{3}He data with minimal uncertainties associated with nuclear corrections.

Estimating all the corrections and their uncertainties we come to the conclusion that in this experiment the statistical error on the final result is still the dominant error.

6 Summary and Beam Request

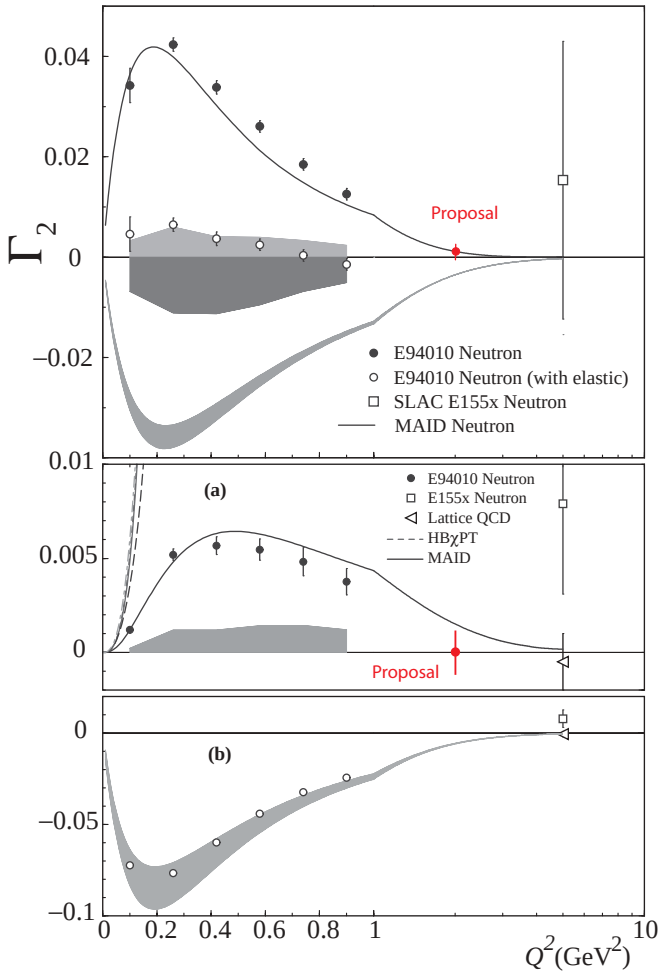

Figure 11: d_2^n and Γ_2^n projected results at $Q^2 = 2$ GeV^2 from this proposal compared to JLab E94-010 and SLAC E155X. Description is similar to that of Fig. 4 and Fig 5.

In summary, we propose to carry out a precision determination of d_2^n. We will determine asymmetries in the region $(0.24 \leq x \leq 0.8)$ (see Fig 11) from a measurement using a high pressure polarized ^{3}He target (P_t= 40%) and the highest available energies (5.7 and 6.0 GeV) of the polarized beam (P_b=80%). This measurement requires 462.2 hours of beam on target for the

measurement of the transverse asymmetry and 155.8 hours for the measurement of the longitudinal asymmetry, along with 60 hours for the beam energy change, spectrometer momentum changes, elastic scattering calibration and beam and target polarization measurements. We therefore request a total of 679 hours (28 days) of beam time to achieve a statistical uncertainty on d_2^n of $\Delta d_2^n \approx 1.18 \times 10^{-3}$ at $Q^2 = 2.0$ GeV^2 in the measured x range.

References

[1] E. Shuryak and A. Vainshtein, Nuc. Phys. B **201** (1982) 141.

[2] R. L. Jaffe and X. Ji, Phys. Rev. D **43** (1991) 724.

[3] B. W. Filippone and X. Ji, Adv. in Nucl. Phys. **26**, 1 (2001).

[4] D. Adams *et al.*, Phys. Lett. **B336** (1994) 125.

[5] P. L. Anthony *et al.*, Phys. Rev. Lett. **71** (1993) 959.

[6] P. L. Anthony *et al.*, Phys. Rev. D **54** (1996) 6620.

[7] K. Abe *et al.*, Phys. Rev. Lett. **76** (1996) 587.

[8] K. Abe *et al.*, Phys. Lett. B **404** (1997) 377.

[9] P. L. Anthony *et al.*, Phys. Lett. B**458** (1999) 529.

[10] X. Ji Nucl. Phys. **B402** (1993) 217.

[11] X. Ji and P. Unrau, Phys. Lett. B **333** (1994) 228.

[12] S. A. Larin and J. A. M. Vermaseren, Phys. Lett. B **259**, 345 (1991) and references therein; S. A. Larin, Phys. Lett. B **334**, 192 (1994).

[13] S. Wandzura and F. Wilczek, Phys. Lett. B **72**, 195 (1977).

[14] F. E. Close and R. G. Roberts, Phys. Lett. B **336**, 257 (1994).

[15] Göckeler *et al.*, Phys. Rev. D **63** 074506 (2001).

[16] X. Ji, in Proceeding of the Workshop on Deep Inelastic scattering and QCD, Editors: JF. Laporte et Y. Sirois Paris, France, 24-28 April, 1995 (ISBN 2-7302-0341-4).

[17] X. Ji and W. Melnitchouk, Phys. Rev. D **56**, 1 (1997).

[18] J. Edelmann, G. Piller, W. Weise, N. Kaiser, Nucl. Phys. A **665** (2000) 125.

[19] S. Simula, M. Osipenko, G. Ricco and M. Tauiti, hep/0205118 and references therein.

[20] SLAC E155: P. L. Anthony *et al.*, Phys. Lett. B **553**, 18 (2003).

[21] H. Burkhardt and W. N. Cottingham, Ann. Phys. **56** (1970) 453.

[22] R. Jaffe, Comments Nucl. Part. Phys. 19 (1990) 239.

[23] I. P. Ivanov *et al.*, Phys. Rep. **320**, 175 (1999).

[24] M. Anselmino, A. Efremov and E. Leader, Phys. Rep. **261**, 1 (1995).

[25] M. Amarian *et al.*, Phys. Rev. Lett. **89**, 242301 (2002).

[26] G. Altarelli, B. Lampe, P. Nason and G. Ridolfi, Phys. Lett. B **334**, 187 (1994).

[27] X. Ji and W. Melnitchouk (private communication)

[28] JLab E97-103 experiment, Spokespeople T. Averett and W. Korsh. see http://hallaweb.jlab.org/physics/experiments/he3/g2/temp/

[29] K. Abe *et al.*, Phys. Rev. D **58** (1998) 112003-1.

[30] S. Wandzura and F. Wilczek, Phys. Lett. B **72** (1977) 195.

[31] JLab E01-012 experiment, Spokespeople N. Liyanage, J. P. Chen and S. Choi.

[32] JLab E01-006 experiment, Spokesperson O. Rondon,

[33] H. Weigel, L. Gamberg, H. Reinhart, Phys. Rev. D**55** (1997) 6910.

[34] M. Wakamatsu, Phys. Lett B **487** (2000) 118.

[35] M. Stratmann, Z. Phys. C **60** (1993) 763.

[36] X. Song, Phys. Rev. D **54** (1996) 1955.

[37] E. Stein, Phys. Lett. B **343** (1995) 369.

[38] B. Ehrnsperger, A Schäfer, Phys. Rev. D **52** (1995) 2709.

[39] I. Balitsky, V. Barun, A. Kolesnichenko, Phys. Lett. B **242** (1990) 245; B **318** (1995) 648 (E).

[40] D. Drechsel, S. Kamalov and L. Tiator, Phys. Rev. D **63**, 114010 (2001).

[41] C. W. Kao, T. Spitzenberg and M. Vanderhaeghen, Phys. Rev. D **67**, 016001 (2003).

[42] M.A. Bouchiat, T.R. Carver and C.M. Varnum, Phys. Rev. Lett. **5** (1960) 373.

[43] N.D. Bhaskar, W. Happer, and T. McClelland, Phys. Rev. Lett. **49** (1982) 25.

[44] W. Happer, E. Miron, S. Schaefer, D. Schreiber, W.A. van Wijngaarden, and X. Zeng, Phys. Rev. A **29** (1984) 3092.

[45] T.E. Chupp, M.E. Wagshul, K.P. Coulter, A.B. McDonald, and W. Happer, Phys. Rev. C **36** (1987) 2244.

[46] K.P. Coulter, A.B. McDonald, W. Happer, T. E. Chupp, and M.E. Wagshul, Nuc. Inst. Meth. in Phys. Res. **A 270** (1988) 90.

[47] N.R. Newbury, A.S. Barton, P. Bogorad, G. D. Cates, M. Gatzke, H. Mabuchi, and B. Saam, Phys. Rev. A **48** (1993) 558.

[48] K.P. Coulter, A.B. McDonald, G.D. Cates, W. Happer, T.E. Chupp, Nuc. Inst. Meth. in Phys. Res. A**276** (1989) 29 .

[49] A. Abragam, Principles of Nuclear Magnetism (Oxford University Press, New York, 1961).

[50] L. Whitlow, SLAC-report-357 (1990).

[51] J. W. Lightbody Jr. and J.S. O'Connell, Computers in Physics **2** (1988) 57.

[52] D. Yu. Bardin and N. M. Shumeiko, Nucl. Phys. B **127** (1977) 1251.

[53] T.V. Kuchto and N. M. Shumeiko, Nucl. Phys. B **219** (1983) 412.

[54] I. V. Akushevich and N. M. Shumeiko, J. Phys. **G**: Nucl. Part. Phys. **20** (1994) 513.

[55] L. W. Mo and Y. S. Tsai, Rev. Mod. Phys. **41** (1969) 205.

[56] Y. S. Tsai, SLAC-PUB-848 (1971).

[57] W. Melnitchouk, G. Piller and A.W. Thomas, Phys. Lett. B **346** (1995) 165; S. A Kulagin, W. Melnitchouk, G. Piller and W. Weise Phys. Rev. C **52** (1995) 932.

[58] J.L. Friar et al., Phys. Rev. C **42** (1990) 2310.

[59] R.M. Woloshyn, Nucl. Phys. A **496** (1989) 749.

[60] C. Ciofi degli Atti, E. Pace and G. Salme, Phys. Rev. C **46** (1992) R1591; C. Ciofi degli Atti, S. Scopetta, E. Pace, G. Salme, Phys. Rev. C **48** (1993) 968;

[61] R.W. Schulze and P.U. Sauer, Phys. Rev. C **48** (1993) 38.

[62] D.F. Geesaman, K. Saito and A.W. Thomas, Ann. Rev. Nucl. Part. Sci. **45** (1995) 337.

[63] I.R. Afnan, F. Bissey and A.W. Thomas, nucl-th/0012081..

[64] E. Leader, A.V. Sidorov and D.B. Stamenov, Int. J. Mod. Phys. A **13** (1998) 5573; Phys. Rev. D **58** (1998) 114028.

[65] I.R. Afnan, F. Bissey, J. Gomez, A.T. Katramatou, W. Melnitchouk, G.G. Petratos and A.W. Thomas, Phys. Lett. B **493** (2000) 36.

[66] F. Bissey, W. Melnitchouk, A. W. Thomas, in preparation; W. Melnitchouk, private communication.

[67] C. Boros, V. Guzey, M. Strikman, A.W. Thomas, hep-ph/0008064

[68] S.A. Kulagin and W. Melnitchouk, in preparation.

[69] S. Scopetta, private communication.